MSJ Experimental Translational Clinical

Original Research Article

Investigating the relationship between multi-scale perfusion and white matter microstructural integrity in patients with relapsing-remitting MS

Multiple Sclerosis Journal–Experimental, Translational and Clinical

July–September 2021, 1–10

DOI: 10.1177/20552173211037002

Nicholas J Sisco[1], Aimee Borazanci[2], Richard Dortch[1] and Ashley M Stokes[1]

Abstract

Background: Multiple sclerosis is characterized by the formation of central nervous system demyelinating lesions with microvasculature inflammation.

Objective: Evaluate how lesion cerebral perfusion relates to white matter microstructural integrity in patients with RRMS using perfusion MRI and myelin-related T_1-weighted to T_2-weighted (T_1w/T_2w) ratios.

Methods: Forty-eight patients with RRMS were imaged with dynamic susceptibility contrast imaging using SAGE (spin- and gradient-echo) to calculate global and capillary-sized perfusion parameters, including cerebral blood flow (CBF), volume (CBV), and mean transit time (MTT). T_1w/T_2w ratios were used to indirectly assess white matter microstructural integrity.

Results: For global perfusion metrics, CBF was reduced 28.4% in lesion regions of interest (ROIs) compared to normal appearing white matter (NAWM), CBV was reduced 25.9% in lesion ROIs compared to NAWM, and MTT increased 12.9%. For capillary perfusion metrics (via spin-echo (SE)), CBF-SE was reduced 35.7% in lesion ROIs compared to NAWM, CBV-SE was reduced 35.2% in lesion ROIs compared to NAWM, and MTT-SE increased 9.1%. Capillary-level CBF was correlated ($\rho = 0.34$, $p = 0.024$) with white matter microstructural integrity in lesion ROIs.

Conclusion: This study demonstrates that lesion perfusion is reduced at both the global and capillary level and capillary-associated hypoperfusion is associated with reduced white matter microstructural integrity in RRMS.

Keywords: Multiple sclerosis, MRI, quantitative MRI, demyelination, relapsing/remitting

Date received: 1 February 2021; accepted: 16 July 2021

Introduction

Myelin and axonal damage that leads to lesion plaques is a hallmark of multiple sclerosis (MS). Relapsing remitting MS (RRMS) is the most common form of MS where episodes present with acute symptoms, e.g., visual loss, neuropathy (numbness/tingling), loss of balance, and muscular atrophy, followed by periods of spontaneous recovery.[1,2] The pathophysiological conditions that lead to RRMS episodes stem from immune system dysregulation leading to acute inflammation and demyelination that form focal lesions. These episodes are followed by resolution of symptoms and sporadic remyelination. Successful remyelination is heterogeneous and depends on patient-specific factors including disease duration, patient age, and other non-MS-related comorbidities.[3–5] Incomplete remyelination results in irreversible axonal loss, chronic deficits, or progression of RRMS, which can ultimately lead to secondary progressive MS resulting in permanent neurological deficits and clinical disability.[2]

Demyelination and lesion formation is associated with breakdown of the blood-brain barrier (BBB) around post capillary venules, where MS lesions are commonly located.[5] BBB permeability leads to the infiltration of lymphocytic cells that disrupt

Correspondence to:
Ashley M Stokes,
Division of Neuroimaging Research, Barrow Neurological Institute, Phoenix, AZ 85013, USA.
Ashley.Stokes@BarrowNeuro.org

Nicholas J Sisco[1]
Aimee Borazanci[2],
Richard Dortch[1],
Ashley M Stokes[1],
[1]Division of Neuroimaging Research, Barrow Neurological Institute, Phoenix, AZ, USA
[2]Department of Neurology, Barrow Neurological Institute, Phoenix AZ USA

myelin sheath integrity[2] and is associated with microvascular perfusion changes.[6,7] Furthermore, adequate cerebral perfusion appears to play a critical role in successful remyelination.[3,5,8,9]

Dynamic susceptibility contrast (DSC) magnetic resonance imaging (MRI) can be used to quantitatively assess cerebral perfusion and can be diagnostic for the acute inflammatory phase of lesion development.[1,10–12] Using DSC-MRI, increases, and decreases, in global perfusion have been observed in MS,[13,14] reflecting the intricate spatiotemporal dynamics and heterogenous disease progression that is characteristic of RRMS. In normal-appearing white matter (NAWM), hypoperfusion has been associated with persistent low-grade inflammation, metabolic or vascular dysfunction, or primary ischemia.[10,14] Conversely, increased perfusion preceding focal WM lesion formation could indicate an increased inflammatory response prior to tissue damage in NAWM.[1] Given these findings and the known relationship between perfusion and myelin repair,[15] the development of biomarker assays that quantitatively probe both cerebral perfusion and myelin is critical to assessing acute inflammatory activity and regenerative potential.

In this study, we investigate the relationship between cerebral perfusion and WM microstructural integrity in patients with RRMS. Given the known microvascular component to MS, a combined spin- and gradient-echo (SAGE) perfusion imaging method was used to obtain complementary global and capillary-sized perfusion metrics,[16–19] including cerebral blood flow (CBF), cerebral blood volume (CBV), and mean transit time (MTT). As quantitative myelin measures are not widely available in clinical settings, the ratio of T_1w to T_2w images has been proposed as a potential biomarker of myelin, though it is recognized that these ratios are impacted by a range of microstructural features.[20,21] Despite these caveats, T_1w/T_2w ratios are influenced by myelin content and serve herein as a sensitive but non-specific biomarker of WM microstructural integrity and damage. Our goal was to assess how SAGE-derived perfusion estimates relate to WM microstructural integrity, which we propose may provide valuable insight into MS disease progression in future studies.

Methods

Patients

This study was performed per the local Institutional Review Board. All participants gave written, informed consent in this HIPAA-compliant study. A total of 79 patients with RRMS were recruited to this study by a practicing neurologist over a period of 18 months, of which 57 were eligible for the study. Inclusion criteria included patients with clinical diagnosis of RRMS between 18 and 55 years of age scheduled for a 3 T brain MRI. Subjects were excluded if they were not scanned with SAGE-DSC ($n = 6$), did not have any lesions ($n = 1$), had orthodontic artifacts ($n = 1$), or were missing dynamic data points ($n = 1$). All patients ($n = 48$) underwent a self-reported quality-of-life assessment using the Functional Assessment of MS (FAMS) questionnaire,[22] followed by MRI.

Image acquisition

MRI was performed at 3.0 T Ingenia (Philips) with a dedicated 13-channel head coil. T_1w images were acquired using magnetization-prepared rapid acquisition gradient-echo (MPRAGE) with repetition time (TR) of 7.9 ms, echo time (TE) of 3.5 ms, field of view (FOV) of $256 \times 256\,mm^2$, in-plane resolution of 0.5×0.5 mm, slice thickness of 1 mm, 170 sagittal slices, and 8° flip angle. T_2w turbo spin-echo (TSE) images were acquired with FOV of $230 \times 230\,mm^2$, in-plane resolution of 0.45×0.45 mm, slice thickness of 5 mm, 30 axial slices, and TR/TE of 4000/148.5 ms. T_2w fluid attenuated inversion recovery (FLAIR) were acquired using the same parameters except TR/TE of 9000/148.5 ms and an inversion time of 2500 ms.

For SAGE-DSC, five echoes (two gradient-echo, 2 asymmetric spin-echo, and 1 spin-echo) were acquired every 1.8 s, with respective TEs of 8.8, 26, 55, 72, and 88 ms for $TE_{1\text{-}5}$. The FOV was $240 \times 240\ mm^2$, with in-plane resolution of 2.5×2.5 mm and 15 slices with slice thickness of 5 mm. After 45 s of baseline images, a standard dose (0.1 mmol/kg) of gadolinium-based contrast agent (Gadobutrol, Gadavist) was injected intravenously at 3 mL/s using a power injector. SAGE-DSC acquisition lasted 4.5 minutes. Following SAGE-DSC, post-contrast T_1w images were acquired using the same parameters as the pre-contrast T_1w images to identify active lesions.

Image processing

Perfusion analysis was performed using in-house MATLAB (MathWorks, Inc) scripts. Much of the background on SAGE and DSC-MRI can be found in a recent review.[23] Dynamic MR signals were converted to relaxation rate time profiles as follows.

The first two gradient-echoes were used to compute ΔR_2* time series according to

$$\Delta R_2^*(t) = \frac{1}{TE_2 - TE_1}\left(\ln\left(\frac{S_{TE_{2,pre}}}{S_{TE_2(t)}}\right) - \ln\left(\frac{S_{TE_{1,pre}}}{S_{TE_1(t)}}\right)\right) \quad (1)$$

where S_{TE2} and S_{TE1} indicate the dynamic signals for TE_1 and TE_2, respectively, and $S_{TE(1\ or\ 2),pre}$ indicates the average pre-bolus signal. From the two gradient-echoes, the signal extrapolated to TE = 0 can be calculated as

$$S_{TE=0} = S_{TE_1}\left(\frac{S_{TE_1}}{S_{TE_2}}\right)^{\frac{TE_1}{(TE_2 - TE_1)}} \quad (2)$$

As previously derived and validated,[18,24] the spin-echo (SE) signal was combined with the T_1-weighted $S_{TE=0}$ to compute the ΔR_2 time-series according to

$$\Delta R_2(t) = \frac{1}{TE_5}\left(\ln\left(\frac{S_{TE_5,pre}}{S_{TE_5}(t)}\right) - \ln\left(\frac{S_{TE=0,pre}}{S_{TE=0}(t)}\right)\right) \quad (3)$$

where TE_5 corresponds to the spin-echo. Perfusion metrics derived from SAGE-DSC acquisition are insensitive to T_1 leakage effects that may occur with MS since T_1 effects are inherently removed from both ΔR_2^* and ΔR_2 using SAGE pulse sequences. The gradient-echo-based ΔR_2^* and spin-echo-based ΔR_2 were subsequently used to quantify global and capillary-sized perfusion, respectively.[23] The ΔR_2^* and ΔR_2 time-courses were converted to contrast agent (CA) concentration using the effective transverse relaxivities.[23] The arterial input function (AIF) was determined from the SAGE ΔR_2^* time courses using automated methods specifically designed for multi-echo acquisitions.[23] Gradient- and spin-echo-based CBV maps were determined from the ratio of the scaled integral between the tissue CA concentration curves and the AIF over 120 s,[23] where negative CA concentrations were not included in the integration to avoid artificially low CBV values.[18] Gradient- and spin-echo-based CBF maps were calculated as the maximum value of the impulse response function determined from deconvolution of the AIF and tissue CA concentration using block-circulant singular value decomposition.[18] Gradient- and spin-echo-based MTT maps were calculated as the ratio of CBV to CBF. Due to the differential vessel size sensitivity of gradient-echo and spin-echo,[23] the capillary-sized-sensitive spin-echo perfusion measures will be referred to with "-SE", e.g., CBF-SE; otherwise the parameter refers to the globally-sensitive gradient-echo, e.g., CBF.

Gray matter standardized T_1w/T_2w (sT_1w/T_2w) ratios were used to assess WM microstructural integrity. To calculate sT_1w/T_2w ratios, T_1w-MPRAGE and T_2w-TSE images were first corrected for bias field inhomogeneities using Advanced Normalization Tools (ANTs, http://stnava.github.io/ANTs/) before brain extraction (BET) and subsequent affine linear registration with FLIRT using the FSL package (https://fsl.fmrib.ox.ac.uk/fsl/). The T_2w image was then scaled to the T_1w image intensities by multiplying the T_2w image by a scaling factor derived from the ratio of median signal intensities in normal-appearing gray matter (NAGM) within each image:[21]

$$sT_2w = \frac{median(T_1w_{NAGM})}{median(T_2w_{NAGM})} \times (T_2w) \quad (4)$$

Using the sT_2w image, the sT_1w/T_2w ratio was then calculated according to

$$\frac{sT_1w}{T_2w} = \frac{T_1w - sT_2w}{T_1w + sT_2w} \quad (5)$$

All images and parametric maps were registered to the T_1w-MPRAGE for statistical analysis. T_1w-MPRAGE and T_2w-FLAIR images were used to obtain lesion regions-of-interest (ROIs) using the lesion segmentation toolbox (LST) that implements a lesion growth algorithm[25] through statistical parametric mapping version 12 (SPM12, https://www.fil.ion.ucl.ac.uk/spm/software/spm12/). Tissue segmentation for NAWM, NAGM, and cerebrospinal fluid (CSF) was performed using the hMRI-toolbox[26] implemented through SPM12. Tissue segmentations were first verified for mutual exclusivity to ensure lesion segmentations were excluded from the NAWM and NAGM segmentations. Next the ROI masks were eroded five times with MATLAB's erode function to yield conservative ROI boundaries free of partial volume effects.

Statistical analysis

The SAGE-DSC parameters and sT_1w/T_2w ratio ROI voxel intensity values are reported as the

median values at the subject level to minimize the impact of extreme values and skew within the ROIs of each subject. Results at the population level are reported as the median voxel intensities of the entire population, with variability reported as the median absolute deviation (MAD). Nonparametric Wilcoxon rank sum tests were used to evaluate pairwise differences in quantitative MRI data across lesion, NAWM, and NAGM ROIs. Associations between WM microstructural integrity (sT_1w/T_2w ratios), perfusion parameters (SAGE metrics), and clinical measures (FAMS, age, and disease duration) were assessed using non-parametric Spearman's correlation, with age and sex as covariates. Correction for multiple comparisons was performed using the false discovery rate (FDR) method, with a threshold for statistical significance of $p < 0.05$. Strength of correlation follows the usual definition, i.e., 0 to 0.2 is "very weak", 0.2 to 0.4 is "weak", and above these are moderate to strong.

Results

SAGE-DSC scans were well tolerated by all patients ($n = 48$). The average age of the cohort was 37.0 ± 9.5, with 73% female participants. The average number of lesions ($\pm$ SD) and lesion volume were 15 ± 13 and $9.5 \pm 14.7\,cm^3$, respectively. The average functional assessment, as measured by the FAMS score, was 117.3 ± 36.1 (0–200; lower scores indicate subjectively lower quality of life). A full summary of the demographics and clinical characteristics can be found in Table 1.

Representative images and SAGE-DSC parameter maps for a single patient (age: 22, female, FAMS: 145) are shown in Figure 1. Two T_2w-hyperintense lesions are visible, as shown by the green arrows. Figure 1(a) to (d) show the standard structural images, namely pre-contrast T_1w, post-contrast T_1w, T_2w-TSE, and T_2w-FLAIR, respectively. Note, none of the patients displayed contrast enhancing lesions assessed through analyzing pre- vs post-contrast T_1w images. Figure 1(e) to (j) demonstrate the SAGE-DSC parameter maps, where Figure 1(e), (g), and (i) reflect global cerebral perfusion and Figure 1(f), (h), and (j) reflect capillary-sensitive perfusion. As expected, contrast between NAGM and NAWM can be seen in the CBF and CBV

Table 1. Demographic and clinical characteristics.

N (female)	48 (35)
Age[a] (yrs.)	37.0 (9.5) (18–55)
Hyperintense lesion count[a]	15 (13) (1–88)
Mean hyperintense lesion volume[a] (cm^3)	9.5 (14.7) (0.2–66.3)
Mean NAWM volume[a] (cm^3)	412.5 (40.4) (333.4–497.3)
Mean NAGM volume[a] (cm^3)	818.5 (75.5) (674.3–980.1)
FAMS score[a]	117.3 (36.1) (46–175)
BMI[a]	29.0 (7.5) (17.5–54)
Race/ethnicity:	
Non-Hispanic/Hispanic or Latino/Not Reported	38/8/2
White/African-American/American Indian/Alaska Native	43/3/2
Most recent steroid use	
<1 month	2
1–6 months	5
>6 months	31
Never	10
Most recent relapse	
<6 months	10
6–12 months	9
1–4 years	16
>4 years/never	13
Disease duration	
<2 years	14
2–5 years	19
>5 years	15

[a]Mean (SD) (range).

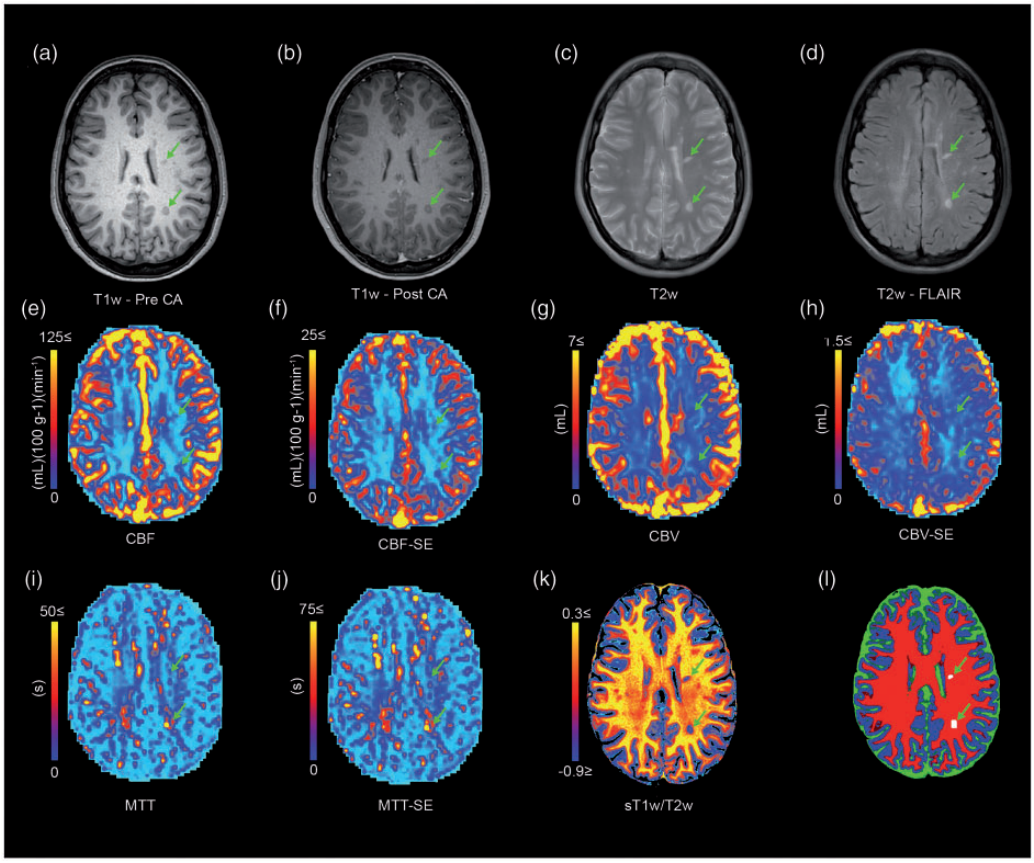

Figure 1. Structural (a–d: T1w-pre contrast, T1w-post contrast, T2w, and T2w-FLAIR) images. Perfusion maps (e–j) are shown with color bar representing the range of perfusion values to enhance visual clarity. The myelin content sT1w/T2w map is shown in K. Tissue segmentation (l) is shown with green as CSF, blue as gray matter, red as NAWM, and white as lesion ROIs. T2w-hyperintense lesions are indicated by the green arrows. Parameter maps, sT1w/T2w, and tissue segmentations are in T1w structural space, but T2w and FLAIR images are shown here in their native space. Panel A show radiological orientations (Right (R)/Left (L)) that applies to each image.

maps; additionally, the magnitude of capillary-sized perfusion values is lower than global perfusion values. Lastly, the sT_1w/T_2w ratio (Figure 1(k)) shows high contrast between NAGM, NAWM, and lesion values. Figure 1(l) shows the representative tissue segmentations.

Median values from each image were calculated for NAWM, NAGM, and lesion ROIs. SAGE-based perfusion parameters showed significant differences between each ROI tissue type (Figure 2(a) to (f)). For sT_1w/T_2w, the only ROIs that were not significantly different were NAGM to lesion ROIs (Figure 2(g)). For both global and capillary-sized perfusion, CBF (Figure 2(a) and (b)) and CBV (Figure 2(c) and (d)) in lesion ROIs were significantly decreased compared to NAGM and NAWM, while lesion MTT (Figure 2(e) and (f)) was significantly increased. Additionally, sT_1w/T_2w (Figure 2 (g)) was significantly lower in lesions compared to NAWM, which reflects changes in WM microstructural integrity within these lesions that could be associated with de/remyelination, axonal loss, or other WM tissue damage. Figure S1 shows the corresponding pairwise plots for each metric and ROI shown in Figure 2.

The population median values are summarized in Table 2 for each metric and ROI. CBF showed a 28.4% reduction in lesion perfusion compared to NAWM (NAWM $= 34.5 \pm 17.9$ vs lesion $= 24.7 \pm 11.9$ mL/100 g/min) and CBF-SE showed a 35.7% reduction (NAWM $= 24.1 \pm 12.1$ vs. lesion $= 15.5 \pm 6.9$ mL/100 g/min). Lesion CBV showed a 25.9% reduction compared to NAWM (NAWM $= 2.7 \pm 1.1$ mL vs. lesion $= 2.0 \pm 0.7$ mL) and CBV-SE lesion ROIs showed a 35.2% reduction relative to NAWM (NAWM $= 1.7 \pm 0.7$ mL vs. lesion $= 1.1 \pm 0.4$ mL). MTT lesion ROIs showed a 12.9% increase in clearance time relative to NAWM

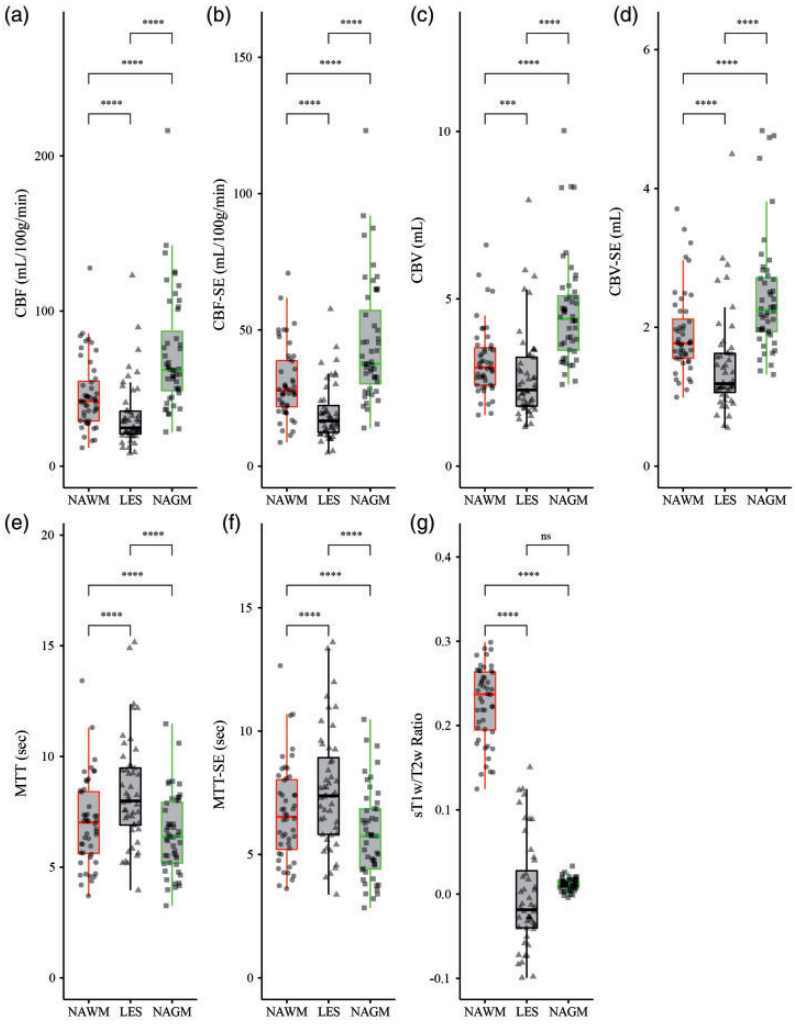

Figure 2. Median values from each SAGE perfusion map and sT1w/T2w ratio in NAWM (red boxes, circles), lesion ROIs (gray boxes, triangles), and NAGM (green boxes, squares). A, C, and E correspond to SAGE perfusion metrics sensitive to all vasculature. B, D, and F correspond to SAGE perfusion metrics sensitive to microvasculature. G corresponds to sT1w/T2w ratio maps. Each tissue ROI per image was compared to each other using pairwise Wilcoxon tests (after FDR p correction, **** indicates $p < 0.0001$; *** indicates $p < 0.001$; ns indicates not significant).

Table 2. Population median (MAD) for each parameter and tissue ROI.

	Tissue median (MAD)		
DSC parameters	NAGM	NAWM	Lesion
CBF ($ml \times (100\,mg)^{-1} \times mL^{-1}$)	45.1 (24.7)	34.5 (17.9)	24.7 (11.9)
CBF-SE ($ml \times (100\,mg)^{-1} \times mL^{-1}$)	30.8 (16.5)	24.1 (12.1)	15.5 (6.9)
CBV (mL)	3.8 (1.6)	2.7 (1.1)	2.0 (0.7)
CBV-SE (mL)	1.9 (0.8)	1.7 (0.7)	1.1 (0.4)
MTT (s)	6.5 (2.4)	7.0 (2.3)	7.9 (2.5)
MTT-SE (s)	5.7 (2.5)	6.6 (2.6)	7.2 (3.0)
sT_1w/T_2w ratio	0.04 (0.16)	0.21 (0.05)	0.00 (0.10)

CBF (SE): cerebral blood flow (spin-echo); CBV (SE): cerebral blood volume (spin-echo); MTT (SE): mean transit time (spin-echo); MAD: median absolute deviation.

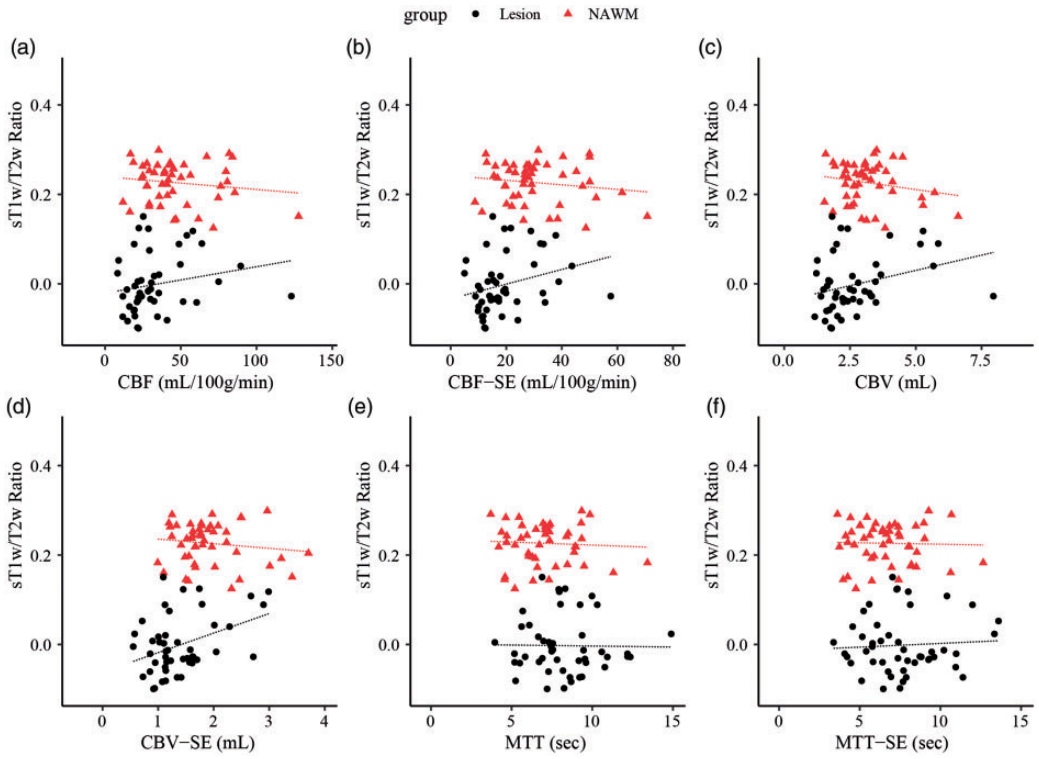

Figure 3. Correlation plots of sT1w/T2w ratios as a function of SAGE-DSC parameter. As with Figure 2(a), (c), and (e) correspond to sT1w/T2w vs total vasculature perfusion and B, D, and F correspond to the sT1w/T2w vs microvasculature perfusion. Our exploratory analysis here shows a positive correlation in CBF-SE and CBV-SE in lesion ROIs. This suggests that decreased myelin content, assessed by sT1w/T2w, is associated with decreased microvascular perfusion. The values of the Spearman rank correlation and *p*-values are summarized in Table 3. CBF-SE was significantly correlated with sT1w/T2w after FDR threshold and accounting for age and sex. Our analysis tested a monotonic relationship with Spearman's correlations; note here we show a fit line on this figure to guide the reader's eye.

(NAWM = 7.0 ± 2.3 s vs. lesion = 7.9 ± 2.5 s) and MTT-SE lesion ROIs showed a 9.1% increase (NAWM = 6.6 ± 2.6 s vs. lesion = 7.2 ± 3.0 s). The sT_1w/T_2w ratios show decreased values in tissues relative to NAWM (NAWM = 0.21 ± 0.05 and lesion = 0.001 ± 0.10).

Correlations between MRI metrics and age, disease duration, and FAMS score are shown in supplementary Figures S2-4, respectively. NAWM CBV ($p = 0.024$) and lesion CBV ($p = 0.02$), CBF ($p = 0.005$), and CBF-SE ($p = 0.02$) were positively correlated with age. No significant trends were noted for disease duration or FAMS score.

Correlations between median sT_1w/T_2w ratio as a function of SAGE-DSC perfusion parameters are shown in Figure 3. Spearman's rank correlation coefficients (ρ) and corresponding *p*-values are summarized in Table 3. Lesion CBF-SE showed a positive significant correlation with sT_1w/T_2w ratios (Figure 3(b), $\rho = 0.33$, $p = 0.024$). Macrovascular CBF, CBV, and microvascular CBV-SE were not significant but had similarly positive trends. None of the other metrics approached significance when correlated with sT_1w/T_2w.

Discussion

This exploratory study investigated the relationship between brain perfusion and WM microstructural integrity in patients with RRMS. An advanced perfusion method was used to quantitatively measure global and capillary-sized CBF, CBV, and MTT in 48 patients with RRMS. Compared to NAWM, lesion ROIs showed significantly reduced perfusion (CBF and CBV) and increased MTT, as well as reduced WM microstructural integrity. Global and capillary-sized perfusion metrics are indicative of hemodynamic changes, and these changes within lesion ROIs were associated with altered WM microstructural integrity from sT_1w/T_2w ratios. WM microstructural integrity displayed weak positive correlations in lesion ROIs with CBF, CBV, CBF-SE, and CBV-SE perfusion parameters (Figure 3,

Table 3. Spearman correlation coefficient and corresponding p-values between sT1w/T2w and perfusion metrics.

DSC-Parameter		CBF	CBF-SE	CBV	CBV-SE	MTT	MTT-SE
Lesion	ρ	0.27	0.33	0.27	0.26	–0.05	–0.02
	p	0.07	**0.024**[a]	0.07	0.08	0.74	0.90
NAWM	ρ	–0.093	–0.03	–0.07	–0.02	–0.003	–0.016
	p	0.54	0.83	0.64	0.89	0.98	0.92

[a]Meets FDR threshold for significance.

Table 3). More broadly, we highlight the feasibility of using SAGE-DSC for assessing comprehensive hemodynamic changes in both global and capillary-sized perfusion in the context of RRMS.

Standard DSC-MRI (single gradient-echo) or arterial spin labeling (ASL) have been used previously in MS perfusion-based studies. Single gradient-echo DSC is sensitive to all vessel sizes and reflects global perfusion. On the other hand, spin-echo DSC is specific to smaller, capillary-sized, vessel perfusion, though this method is less commonly used. ASL perfusion measurements have the benefit of not requiring contrast agents but suffer from low signal-to-noise ratios complicating analysis. Using multiple echoes and contrasts, SAGE-based perfusion imaging provides data on both global and capillary-sized cerebral perfusion. Previously, SAGE-DSC was used to study brain tumors with improved perfusion accuracy,[18,19,24,27] and in stroke where capillary sensitivity can improve microinfarct conspicuity.[16] In the context of MS, inclusion of SAGE-DSC could provide valuable cerebral perfusion parameters by combining the high signal-to-noise ratio of gradient-echo signals with the microvascular specificity from spin-echo signals, which could contribute to MRI-based diagnosis and monitoring. Additionally, SAGE-MRI perfusion measurements are insensitive to T_1 leakage effects that may occur in MS.

Using SAGE-DSC, we show that small vessel perfusion alterations are associated with changes in WM microstructural integrity. To our knowledge, the relationship between cerebral perfusion alterations and WM microstructural integrity has not previously been quantified in the context of RRMS. Active demyelination is associated with a complex pro-inflammatory cascade that has been shown to correlate negatively with CBF alterations.[28] A recent study in healthy cognitively unimpaired adults showed a correlation between CBF and myelin water fraction (MWF)[29] such that as WM microstructural integrity decreased, concomitant decreases in CBF were observed. We found a correlation between capillary-sized cerebral perfusion metrics and WM microstructural integrity assessed using sT_1w/T_2w ratios. These concomitant changes may reflect different stages of demyelination or remyelination; alternatively, we acknowledge that other effects, including gliosis or secondary changes, could simultaneously affect these measurements. Future studies should investigate whether perfusion changes are indicative of remyelination or demyelination processes.

There are several limitations in this study. As this is a pilot study in a relatively small population, our population did not include healthy controls or patients in acute phase, and we were unable to control for lifestyle factors, e.g., exercise, smoking, caffeine intake, or specific medications like amphetamine or corticosteroids that are known to alter perfusion measurements. Secondly, sT_1w/T_2w ratios are not a quantitative myelin biomarker, as it is derived from the ratio of images with arbitrary units of intensity scaling and is further limited by the inherent underlying sensitivities of T_1w and T_2w images to the effects of edema and iron content. Given this, future work will focus on comparing SAGE perfusion estimates to more specific myelin measures (e.g., magnetization transfer, myelin water imaging).[30] Additionally, SAGE-DSC as implemented here does not have full brain coverage due to the inclusion of the SE; future studies will implement simultaneous multi-slice approaches to ensure whole brain SAGE-DSC coverage. Additionally, cortical lesions can go undetected due to their small size, which may affect the true perfusion values in our data. The perfusion values used in this study may not reflect the true CBF or CBV due to the unknown spin- and gradient-echo proportionality constants (i.e., relaxivities) used to calculate the CBF and CBV,[23] which is an active area of

research in our lab. Future research on multiple timepoints, larger populations, and more quantitative myelin measurements may further corroborate the link between adequate perfusion and myelin.

Conclusion

In this exploratory study, global and capillary-sized perfusion metrics derived from SAGE-DSC were compared across lesion, NAWM, and NAGM. Combining these metrics with a marker of WM microstructural integrity, we posit that this approach may be a useful approach to measure inflammatory processes associated with demyelination. More studies on the relationship between SAGE-based cerebral perfusion (both at the global and capillary level) and metrics specific for myelin microstructural integrity are needed.

Acknowledgements

The authors thank Charrid Simpson, RN, MSN, FNP-C, MSCN, and Ashley Nespodzany, MS, for help with patient recruitment, and Maurizio Bergamino, Ph.D., and Laura Bell, Ph.D., for many helpful discussions.

Conflict of Interests

The author(s) declared no potential conflicts of interest with respect to the research, authorship, and/or publication of this article.

Funding

The author(s) disclosed receipt of the following financial support for the research, authorship, and/or publication of this article: This work was supported by the Barrow Neurological Foundation and NIH R01NS097821.

ORCID iD

Nicholas J Sisco https://orcid.org/0000-0003-2091-868X

Supplemental Material

Supplemental material for this article is available online.

References

1. Peruzzo D, Castellaro M, Calabrese M, et al. Heterogeneity of cortical lesions in multiple sclerosis: an MRI perfusion study. *J Cereb Blood Flow Metab* 2013; 33: 457–463.
2. Filippi M, Bar-Or A, Piehl F, et al. Multiple sclerosis. *Nat Rev Dis Prim* 2018; 4: 43.
3. Chari DM. Remyelination In Multiple Sclerosis. *Int Rev Neurobiol* 2007; 79: 589–620.10.1016/S0074-7742(07)79026-8.
4. Hagemeier K, Bruck W and Kuhlmann T. Multiple sclerosis – remyelination failure as a cause of disease progression. *Histol Histopathol* 2012; 27: 277–287.
5. Filippi M, Brück W, Chard D, et al.; Attendees of the Correlation between Pathological and MRI findings in MS workshop. Association between pathological and MRI findings in multiple sclerosis. *Lancet Neurol* 2019; 18: 198–210.
6. Lin Y, Pan Y, Wang M, et al. Bloodbrain barrier permeability is positively correlated with cerebral microvascular perfusion in the early fluid percussion-injured brain of the rat. *Lab Invest* 2012; 92: 1623–1634.
7. Law M, Saindane AM, Ge Y, et al. Microvascular abnormality in relapsing-remitting multiple sclerosis: perfusion MR imaging findings in normal-appearing white matter. *Radiology* 2004; 231: 645–652.
8. Holland CM, Charil A, Csapo I, et al. The relationship between normal cerebral perfusion patterns and white matter lesion distribution in 1,249 patients with multiple sclerosis. *J Neuroimaging* 2012; 22: 129–136.
9. Pohl HB, Porcheri C, Mueggler T, et al. Genetically induced adult oligodendrocyte cell death is associated with poor myelin clearance, reduced remyelination, and axonal damage. *J Neurosci* 2011; 31: 1069–1080.
10. Ge Y, Law M, Johnson G, et al. Dynamic susceptibility contrast perfusion MR imaging of multiple sclerosis lesions: characterizing hemodynamic impairment and inflammatory activity. *Am J Neuroradiol* 2005; 26: 1539–1547.
11. Lapointe E, Li DKB, Traboulsee AL, et al. What have we learned from perfusion MRI in multiple sclerosis? *AJNR Am J Neuroradiol* 2018; 39: 994–1000.
12. Sheng H, Zhao B and Ge Y. Blood perfusion and cellular microstructural changes associated with iron deposition in multiple sclerosis lesions. *Front Neurol* 2019; 10: 1–10.
13. Bester M, Forkert ND, Stellmann JP, et al. Increased perfusion in normal appearing white matter in high inflammatory multiple sclerosis patients. *PLoS One* 2015; 10: e0119356.
14. Sowa P, Bjornerud A, Nygaard GO, et al. Reduced perfusion in white matter lesions in multiple sclerosis. *Eur J Radiol* 2015; 84: 2605–2612.
15. Mahad DH, Trapp BD and Lassmann H. Pathological mechanisms in progressive multiple sclerosis. *Lancet Neurol* 2015; 14: 183–193.
16. Schmiedeskamp H, Straka M, Newbould RD, et al. Combined spin- and gradient-echo perfusion-weighted imaging. *Magn Reson Med* 2012; 68: 30–40.
17. Schmiedeskamp H, Straka M and Bammer R. Compensation of slice profile mismatch in combined spin- and gradient-echo echo-planar imaging pulse sequences. *Magn Reson Med* 2012 ; 67: 378–388.
18. Stokes AM and Quarles CC. A simplified spin and gradient echo approach for brain tumor perfusion imaging. *Magn Reson Med* 2016; 75: 356–362.
19. Stokes AM, Skinner JT and Quarles CC. Assessment of a combined spin- and gradient-echo (SAGE)

DSC-MRI method for preclinical neuroimaging. *Magn Reson Imaging* 2014; 32: 1181–1190.
20. Pareto D, Garcia-Vidal A, Alberich M, et al. Ratio of T_1-weighted to T_2-weighted signal intensity as a measure of tissue integrity: comparison with magnetization transfer ratio in patients with multiple sclerosis. *AJNR Am J Neuroradiol* 2020; 41: 461–463.
21. Cooper G, Finke C, Chien C, et al. Standardization of T_1w/T_2w ratio improves detection of tissue damage in multiple sclerosis. *Front Neurol* 2019; 10: 1–10.
22. Preedy VR (2011) Functional Assessment Multiple Sclerosis. In: Kreutzer J.S., DeLuca J., Caplan B. (eds) *Encyclopedia of Clinical Neuropsychology*. Springer, New York, NY. https://doi.org/10.1007/978-0-387-79948-3_1809
23. Quarles CC, Bell LC and Stokes AM. Imaging vascular and hemodynamic features of the brain using dynamic susceptibility contrast and dynamic contrast enhanced MRI. *Neuroimage* 2019; 187: 32–55.
24. Stokes AM, Skinner JT, Yankeelov T, et al. Assessment of a simplified spin and gradient echo (sSAGE) approach for human brain tumor perfusion imaging. *Magn Reson Imaging* 2016; 34: 1248–1255.
25. Schmidt P, Gaser C, Arsic M, et al. An automated tool for detection of FLAIR-hyperintense white-matter lesions in multiple sclerosis. *Neuroimage* 2012; 59: 3774–3783.
26. Tabelow K, Balteau E, Ashburner J, et al. hMRI – a toolbox for quantitative MRI in neuroscience and clinical research. *Neuroimage* 2019; 194: 191–210.
27. Newton AT, Pruthi S, Stokes AM, et al. Improving perfusion measurement in DSC-MR imaging with multiecho information for arterial input function determination. *AJNR Am J Neuroradiol* 2016; 37: 1237–1243.
28. Choi B-RR, Kim D-HH, Back D, Bin, et al. Characterization of white matter injury in a rat model of chronic cerebral hypoperfusion. *Stroke* 2016; 47: 542–547.
29. Bouhrara M, Alisch JSR, Khattar N, et al. Association of cerebral blood flow with myelin content in cognitively unimpaired adults. *BMJ Neurol Open* 2020; 2: e000053.
30. Mancini M, Karakuzu A, Cohen-Adad J, et al. An interactive meta-analysis of MRI biomarkers of myelin. *Elife* 2020; 9: e61523.